Interfacial Damage of Fiber/Matrix Composite under Mechanical and Physical Loading

Varbinka Valeva, Jordanka Ivanova, Ana Yanakieva

Abstract— **In this paper on the base of representative volume element (RVE) the modified shear lag model was used to investigate the stress state, stress transfer and interface fracture energy of nanofiber/matrix composite. The RVE is subjected to static mechanical and physical load, e.g. temperature and moisture excitation. The solution of the problem is considered for the cases of perfect bond of the interface, perfect bond and break of the fiber, perfect bond and partially interface debonding and break of the fiber as well. The obtained in closed analytical form results for axial stress and shear interfacial stress as well as the debond length are illustrated in figures. As a numerical example, the carbon nanofiber (CNF)/epoxy composite is considered. Three cases are studied: elastic with static mechanical loading, elastic with static mechanical loading and temperature and elastic with static mechanical loading with temperature and moisture. All three cases are compared in respective figures. The presence of the initial partial debond leads to smaller values of the respective fiber axial and interface shear stresses as well as to the magnitude of the plateau of the axial fiber stress. As a consequence, the progressive interfacial debonding is considered as well. The influence of the temperature excitation (20^o–30^oC) at given characteristics of the chosen CNF composite on the interface debond length is negligible, while the influence of moisture is significant especially for the case of progressive interface debonding. It is shown that the influence of the moisture on CNF is bigger at smaller volume fraction. At smaller aspect ratio (AR) the values of the stress transfer function (STF) are smaller when the influence of the moisture is taken into account and further it increases with the increasing of the mechanical load. The influence of the temperature and moisture on the debonding length is also estimated and some conclusions and recommendations are done.**

Index Terms— **fiber/matrix composite, shear lag model, interface debond length, temperature and moisture excitation**

I. INTRODUCTION

In the last century the reinforced composite successfully took place in different industrial applications. When the nanotechnology proposed as reinforcements of polymer and metal/ceramic matrix (CFRC) the nanoparticles, nanotubes and nanofibers, the interest of the scientific community extremely increases and was directed to experimental and modeling activities. The main problem there is the damage behavior of the reinforcement embedded in the matrix. The different thermal and elastic characteristics of both consistent of the composite lead to appearance of interface damage, known as interface delamination, fiber break, matrix crack [1.2]. So, the adhesion between fiber and matrix requires adequate understanding of damage behavior, Based on the micro and macro experimental techniques for measuring the adhesion between fibers and matrices in composites one can estimate for example the effect of fiber surface treatment on the interfacial shear strength for the cases of the single-fiber pull-out [3], the single-fiber fragmentation [4, 5] and the micro-indentation test [6]. All techniques can serve for different applications. For example, the single-fiber fragmentation test is practically used for characterization of the fiber-matrix interfacial toughness (strength) in composite materials.

On the base of the experimental data and conclusions on the transfer mechanism in CFRC, the analytical modeling [7] and numerical simulations can help in the understanding the analysis of these materials, reducing and optimizing the design and cost of considered composite materials. According to [8], the analysis of the representative volume element (RVE) model is the first step in analyzing the CFRC [8]. In [9] the RVE of a simplified 3D model for a wavy carbon nanotube (CNT) have been considered to study the stress transfer in reinforced composites. The proposed model can predict axial as well as interfacial shear stresses along a wavy CNT embedded in a matrix. The influence of the interfacial debonding along the fibers on the effective moduli of CNT-reinforced composites was studied by a simple analytical model [10]. Based on Mori-Tanaka approach a new improved interface model is proposed, that includes the nanoparticle geometry and clustering effects [11]. Lui and Xu [12] using boundary element method (BEM) to investigate the curved cracks at the interphases between the fiber and matrix and to calculate the stress intensity factors (SIFs). In [13] the influence of the geometry of carbon nanotubes (CNTs on the macroscopic stiffness and microscopic stresses of CNT reinforced polymer composites is estimated on the base of on the multi-scale homogenization theory. In the extensive review [14], the investigations done by the experiments and theory of micronanomechanics as well as numerical analysis on characterizing mechanical properties of nanocomposites is presented and discussed.

The constant shear lag model [15] is one of the most used analytical method to study the transfer mechanism in reinforced composites. The reduction scheme (given in [16]) from 2D to 1D elastic problem is based on the classical shear lag model proposed in [15]. This model and its further modifications [17-18] shows the large applications and good efficiency comparing with various numerical methods.

In this paper on the base of Representative Volume Element (RVE) the shear lag model is used to investigate the stress state, stress transfer and interface fracture energy in CNF/matrix composite, subjected to mechanical loading under influence of environmental physical conditions such as temperature and moisture. The obtained in closed analytical

Varbinka Valeva, Solid Mechanics, Institute of Mechanics, Bulgarian Academy of Sciences, Sofia, Bulgaria.
Jordanka Ivanova, Solid Mechanics, Institute of Mechanics, Bulgarian Academy of Sciences, Sofia, Bulgaria.
Ana Yanakieva, Solid Mechanics, Institute of Mechanics, Bulgarian Academy of Sciences, Sofia, Bulgaria.

form results for axial stress, shear interfacial stress and debond length as well as the STF and fracture energy are illustrated in figures and discussed. The presence of initial partial interface debonding is included in further analytically calculated progressive interface debonding. The effect of aspect ratio, volume fraction and the presence of initial interface debond are also discussed. The novelty of this work is the influence of environment conditions on interfacial damage of CNF composites.

II. State and Solution of the Problem

A. Shear Lag Model

Taking into account the periodicity of such a composite material, a stress-strain behavior of the RVE shown in Fig. 1 under applied tensile stress σ_0 is under consideration. The nanofiber/matrix interface is perfect bonded or particularly debonded. A carbon nanofiber with a length $2l$ and radius r is embedded in the matrix material with a width $2(R-r)$. On Fig. 1 d denotes the given initial debond and l_d - the debond length obtained after applying the load σ_0. Due to the symmetry, only a quarter of the RVE is considered.

The environmental influence such as temperature and moisture excitation, the presence of initial debond length and fiber break are considered additionally of [18].

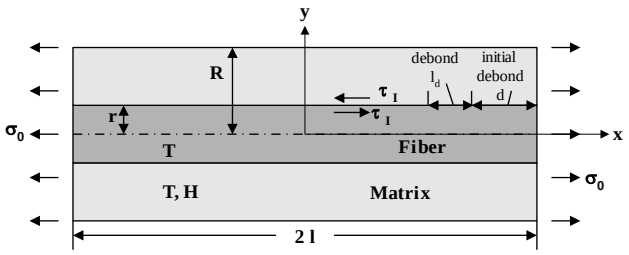

Fig. 1. Representative volume element

The following system of differential equations for the equilibrium of the RVE is given as follows:

$$\frac{\partial \sigma_k}{\partial x}+\frac{\partial \tau_k}{\partial y}=0 \quad (\kappa=f,m)$$
$$\frac{d^2T_\kappa}{dx^2}=0 \qquad \frac{d^2H_m}{dx^2}=0 \tag{1}$$

where σ_k, τ_k ($\kappa=f$ - nanofiber, $\kappa=m$ - matrix) are the axial and shear stress and $\tau_m\big|_{y=r}=\tau_f\big|_{y=r}=\tau_I$, T and H are the temperature and moisture, respectively. The constitutive equations are:

$$\sigma_f=E_f\left\{\frac{\partial u_f}{\partial x}-\alpha_f\left[T_0+(T-T_0)\frac{x}{l}\right]\right\}$$
$$\sigma_m=E_m\left\{\frac{\partial u_m}{\partial x}-\alpha_m\left[T_0+(T-T_0)\frac{x}{l}\right]-\right.$$
$$\left.-\beta_m\left[H_0+(H-H_0)\frac{x}{l}\right]\right\} \tag{2}$$
$$\tau_\kappa=\frac{E_\kappa}{2(1+\nu_\kappa)}\frac{\partial u_\kappa}{\partial y} \quad (\kappa=f,m)$$

where u_κ is the displacement, E_κ is the Young's modulus, ν_κ is the Poisson's ratio $(\kappa=f,m)$ and α_m is the coefficient of thermal expansion of the matrix.

Here and bellow the following notations are used: $\tau_{xy}^\kappa=\tau_\kappa$, $\sigma_x^\kappa=\sigma_\kappa$, $u_x^\kappa=u_\kappa$, $(\kappa=f,m)$, $\sigma_f\big|_{y=r}=\sigma_f^r=\sigma_f$, $\sigma_m\big|_{y=r}=\sigma_m^r$, $\sigma_m\big|_{y=R}=\sigma_m^R$, $u_m\big|_{y=R}=u_m^R, u_m\big|_{y=r}=u_m^r$.

Boundary and contact conditions are given bellow:

- boundary conditions:

$$\sigma_f\big|_{x=l}=\sigma_m\big|_{x=l}=\sigma_0$$
$$\tau_I\big|_{x=0}=0 \qquad \tau_m\big|_{y=R}=0,$$
$$T_k(0)=T_0 \qquad T_k(l)=T \qquad (\kappa=f,m) \tag{3}$$
$$H_m(0)=H_0 \qquad H_m(l)=H$$

- contact conditions:

$$u_f\big|_{y=r}=u_m\big|_{y=r}$$
$$\sigma_m\big|_{y=r}=\xi\sigma_f+\eta \qquad \xi=\frac{E_m}{E_f}$$
$$\eta==E_m\left\{(\alpha_m-\alpha_f)\left[T_0+(T-T_0)\frac{x}{l}\right]+\right. \tag{4}$$
$$\left.+\beta_m\left[H_0+(H-H_0)\frac{x}{l}\right]\right\}$$

Integrating the equilibrium equation (1) with respect y from 0 to r we obtain:

$$\frac{\partial \sigma_f}{\partial x}=-\frac{2\tau_i}{r} \tag{5}$$

The equilibrium equation (1) for matrix gives:

$$\frac{\partial \tau_m}{\partial y}=-\frac{\partial \sigma_m}{\partial x} \tag{6}$$

Solution of (5) for two boundaries $y = r$ and $r \le y < R$ provides the shear stress in matrix:

$$\tau_m = -\frac{\partial \sigma_m}{\partial x} y + C$$

$$\tau_m\big|_{y=R} = 0 \quad \Rightarrow \quad C = R\frac{\partial \sigma_m}{\partial x}$$

i.e.

$$\tau_m = (R-y)\frac{\partial \sigma_m}{\partial x} \tag{7}$$

$$\tau_m\big|_{y=r} = \tau_i = (R-r)\frac{\partial \sigma_m}{\partial x} \;\rightarrow\; \frac{\partial \sigma_m}{\partial x} = \frac{\tau_i}{(R-r)} \tag{8}$$

From (7) and (8) we get a following relation:

$$\tau_m = \frac{R-y}{R-r}\tau_i \tag{9}$$

From (8) and (13) we have:

$$\frac{E_m}{2(1+\nu_m)}\frac{\partial u_m}{\partial y} = \frac{R-y}{R-r}\tau_i \tag{10}$$

Integrating both side of (10) with respect to y from r to R we have τ_i in terms of displacement:

$$\tau_i = \frac{E_m}{(R-r)(1+\nu_m)}\left(u_m^R - u_m^r\right) \tag{11}$$

Substituting (11) into (9) we also have:

$$\tau_m = \frac{(R-y)}{(R-r)^2}\frac{E_m}{(1+\nu_m)}\left(u_m^R - u_m^r\right) \tag{12}$$

The displacement u_m can be derived from (10) and (12):

$$u_m = u_m^r + \frac{2Ry - y^2 + \left(r^2 - 2rR\right)}{(R-r)^2}\left(u_m^R - u_m^r\right) \tag{13}$$

Differentiating (13) with respect to x and multiplying by E_m we have:

$$\sigma_m = \sigma_m^r + \frac{2Ry - y^2 + \left(r^2 - 2rR\right)}{(R-r)^2}\left(\sigma_m^R - \sigma_m^r\right) \tag{14}$$

The equilibrium equation for the stresses in the RVE has the form:

$$r\,\sigma_f + \int_r^R \sigma_m dy = R\,\sigma_0 \tag{15}$$

From (14) and (15) we have:

$$\left(\sigma_m^R - \sigma_m^r\right) = \frac{3\left(R\,\sigma_0 - r\,\sigma_f\right)}{2(R-r)} - \frac{3}{2}\left(\xi\sigma_f + \eta\right) \tag{16}$$

Combining (5) and (11) and substituting (16) we obtain:

$$\frac{d^2\sigma_f}{dx^2} - \frac{3\left[r + (R-r)\xi\right]}{r(R-r)^2\,(1+\nu_m)}\sigma_f = -\frac{3R\sigma_0}{r(R-r)^2\,(1+\nu_m)}\left[R\sigma_0 + (R-r)\eta\right] \tag{17}$$

The solution of (17) is:

$$\sigma_f = A_1 ch(\lambda x) + A_2 sh(\lambda x) + \frac{Ax + B}{\lambda^2}$$

$$\tau_i = -\frac{\lambda r}{2}\left\{A_1 sh(\lambda x) + A_2 ch(\lambda x) + \frac{A}{\lambda^3}\right\} \tag{18}$$

where

$$\lambda = \sqrt{\frac{3\left[r + \xi(R-r)\right]}{r(R-r)^2\,(1+\nu_m)}}$$

$$A = \frac{3E_m}{rl(R-r)\,(1+\nu_m)}\left[\left(\alpha_m - \alpha_f\right)(T - T_0) + \beta_m(H - H_0)\right]$$

$$B = \frac{3R\sigma_0}{r(R-r)^2\,(1+\nu_m)} - \frac{3E_m}{r(R-r)\,(1+\nu_m)}\left[\left(\alpha_m - \alpha_f\right)T_0 + \beta_m H_0\right] \tag{19}$$

Coefficients A_1 and A_2 can be determined using the following boundary conditions:

- for perfect bond on the interface $(0 \le x \le l)$

$$\sigma_f\big|_{x=l} = \sigma_0 \qquad \tau_i\big|_{x=0} = 0 \qquad A_2 = -\frac{A}{\lambda^3}$$

$$A_1 = \frac{1}{ch(\lambda l)}\left[\sigma_0 + \frac{A}{\lambda^3}sh(\lambda l) - \frac{Al + B}{\lambda^2}\right] \tag{20}$$

- for perfect bond on the interface $(0 \le x \le l)$ and fiber break

$$\sigma_f\big|_{x=l} = 0 \qquad \tau_i\big|_{x=0} = 0 \qquad A_2 = -\frac{A}{\lambda^3}$$

$$A_1 = \frac{1}{ch(\lambda l)}\left[\frac{A}{\lambda^3}sh(\lambda l) - \frac{Al + B}{\lambda^2}\right] \tag{21}$$

- for perfect bond $(0 \le x \le l-d)$ and partially debond $(l-d < x \le l)$ on the interface

$$\sigma_f\big|_{x=l-d} = \sigma_0 \qquad \tau_i\big|_{x=0} = 0 \qquad A_2 = -\frac{A}{\lambda^3}$$

$$A_1 = \frac{1}{ch[\lambda(l-d)]}\left[\sigma_0 + \frac{A}{\lambda^3} sh[\lambda(l-d)] - \right. \qquad (22)$$
$$\left. - \frac{A(l-d)+B}{\lambda^2}\right]$$

- for perfect bond $(0 \le x \le l-d)$ and partially debond $(l-d < x \le l)$ on the interface and fiber break

$$\sigma_f\big|_{x=l-d} = 0 \qquad \tau_i\big|_{x=0} = 0 \qquad A_2 = -\frac{A}{\lambda^3}$$

$$A_1 = \frac{1}{ch[\lambda(l-d)]}\left[\frac{A}{\lambda^3} sh[\lambda(l-d)] - \right. \qquad (23)$$
$$\left. - \frac{A(l-d)+B}{\lambda^2}\right]$$

Length of debond l_d can be found from the condition: $\tau_i(x_d) = \tau^{cr}$

$$l_{d_{1,2}} = l - \frac{1}{\lambda}\ln\frac{-Q \pm \sqrt{Q^2 - PR}}{P}$$

$$P \neq 0\,, \quad Q^2 - PR \ge 0\,, \quad \frac{-Q \pm \sqrt{Q^2 - PR}}{P} \ge 1 \qquad (24)$$

$$P = A_1 + A_2\,, \quad Q = \frac{2\tau^{cr}}{\lambda a} + \frac{A}{\lambda^3}\,, \quad R = A_2 - A_1$$

B. *Stress Transfer Function*

The stress transfer function is defined as the fiber axial stress which is integrated over the fiber length and normalized in order to make stress transfer function independent of fiber length [16]:

$$STF = 2\left(\frac{1}{2l}\int_0^l \sigma_f(x)dx\right) \qquad (25)$$

C. *Interface Fracture Energy*

The interface fracture energy is defined as the energy per unit area needed to break the fiber/matrix interface.

The approach proposed in [19, 20] will be applied in present analysis to determine the interface fracture energy in the presence of an initial debond at the fiber/matrix interface. The strain energy for fully-bonded ($U_f^{full-bonding}$), and partially-debonded ($U_f^{partial-bonding}$) fiber/matrix interface is determined following [21]:

$$U_f^{full-bonding} = 2\left(\frac{\pi r^2}{2E_f}\int_0^l (\sigma_f^{full-bonding})^2 dx\right) \qquad (26)$$

$$U_f^{partial-bonding} = 2\left(\frac{\pi r^2}{2E_f}\int_0^l (\sigma_f^{partial-bonding})^2 dx\right) \qquad (27)$$

and the expression for the interface fracture energy has the form:

$$\Gamma_i = \frac{1}{2\pi r d}\left(U_f^{full-bonding} - U_f^{partial-bonding}\right) \qquad (28)$$

where d is the initial debond length.

III. Numerical Example and Results

As a numerical example a RVE (Fig.1) is considered at following conditions: fiber break, full bonded interface and partially bonded interface (the initial debond exists). The RVE has the following geometrical, loading, and environmental characteristics:

$l = 50\,nm$, $r = 1\,nm$, $R = 10\,nm$, $\sigma_0 = 0.5\,GPa$

$\tau^{cr} = 16\,MPa$, $T_0 = 20^0 C$, $T = 40^0 C$

$H_0 = 0.001\,wtr.\%$, $H = 10\,wtr.\%$

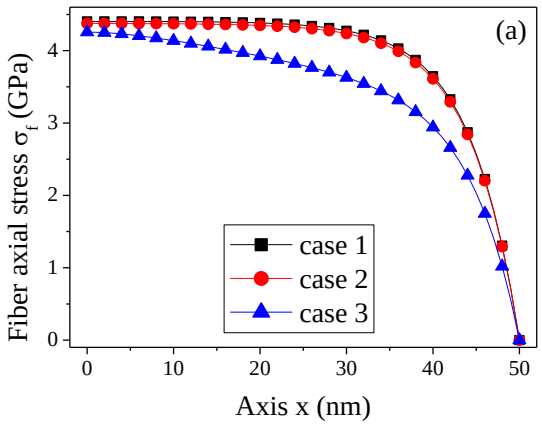

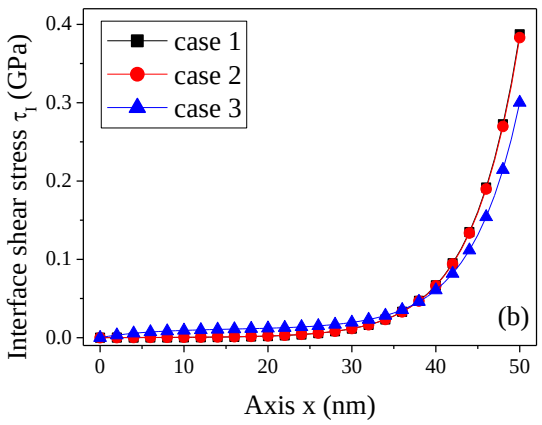

Fig. 2. Fiber axial (a) and interface shear (b) stresses along the fiber length

The characteristics of materials are given in Table I.
The following cases are considered:

case 1: elastic problem

$$\alpha_f = 0, \quad \beta_f = 0, \quad \alpha_m = 0, \quad \beta_m = 0$$

case 2: thermo-elastic problem

$$\alpha_f \neq 0, \quad \beta_f = 0, \quad \alpha_m \neq 0, \quad \beta_m = 0$$

case 3: hygro-thermo-elastic problem

$$\alpha_f \neq 0, \quad \beta_f = 0, \quad \alpha_m \neq 0, \quad \beta_m \neq 0$$

Table I. Mechanical properties of materials [22]

Property	Carbon fiber	Epoxy matrix
Young's modulus (GPa)	276	4.14
Poisson's ratio	0.33	0.36
Coefficient of thermal expansion ($1/^oC$)	$7.2x10^{-6}$	$45x10^{-6}$
Coefficient of moisture expansion (1/wtr. %)	0	$3.24x10^{-3}$

The behavior of the axial fiber stress and interfacial shear stress along the fiber length is shown in Fig. 2. As expected, the maximum axial stress is in the middle of the fiber and it is determined as a saturated point. The maximum shear stress is at the fiber end (singularity of interface shear stress) and tends to zero at the middle of the fiber. The size of plateau of axial fiber stress increases and the maximum values of interface shear stress increase when the moisture is taken into account.

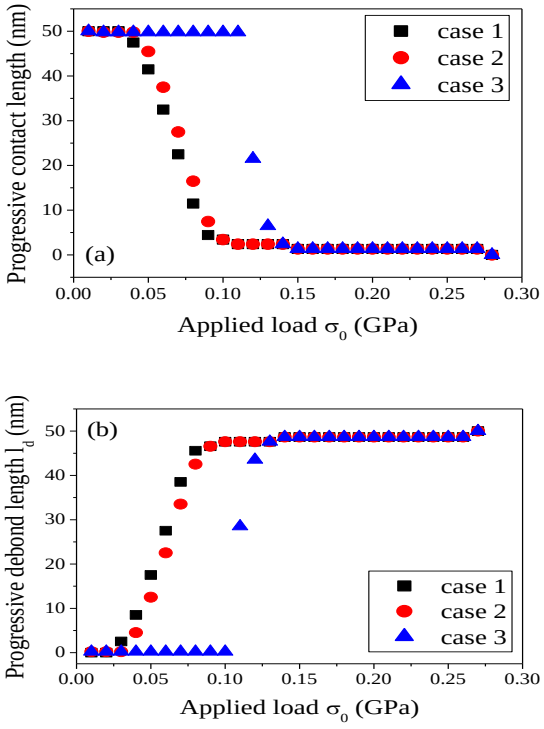

Fig. 3. Progressive contact (a) and debond (b) length for monotonically increasing static load

The interface progressive debond length and respective intact zones for the case of monotonically increasing static loading taking into account the previous debond lengths as initial ones are shown in Fig. 3. In fact if the function debond length-loading is taken as a basic one, the curve for intact zone of the fiber is the inversion function to the basic. This result is reasonable from engineering point of view, but must be proved, which was done.

It has to be pointed out (Fig. 3) that the value of debond length is smaller in the case of the presence of temperature and moisture excitation (case 2 and case 3). For the case 3 it can be seen that after some value of the mechanical load the interface debonding appears suddenly with a bigger length, comparing with cases 1 and 2.

A. Effect of Aspect ratio (AR)

The aspect ratio is defined as the ratio of CNF length to its assumed diameter. Further on, the diameter is assumed to be constant but its length is assumed variable.

Fig. 4 shows the influence of CNF aspect ratio on the fiber axial and interfacial shear stresses. The stress distribution plots are very similar in both the cases. With the increase of aspect ratio, the rate of CNF axial stress and the length of the saturation plateau become higher. The presence of moisture leads to decreasing/absence of the plateau at a small AR.

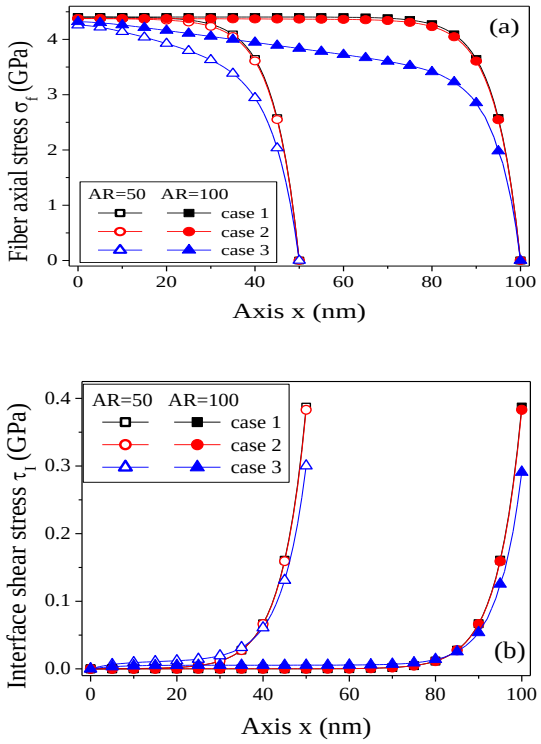

Fig. 4. Effect of aspect ratio on the axial fiber (a) and interface shear (b) stresses distribution

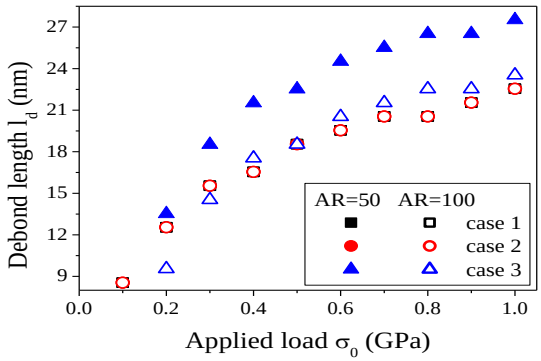

Fig. 5. Effect of aspect ratio on debond length for different values of the mechanical load

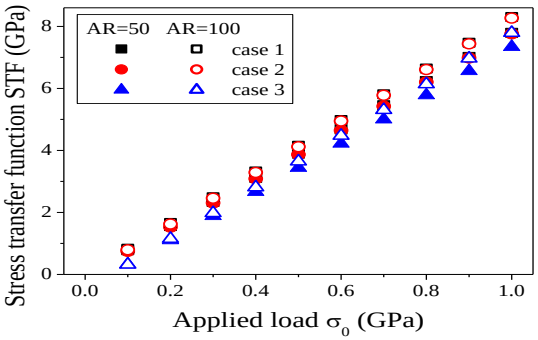

Fig. 6. Effect of aspect ratio on STF for different values of the mechanical load

Coming to Fig. 5 one can see the dependence of the interface debond length on the external loading with/without temperature and moisture for two values of AR. Very clear is the increasing of the debond length with decreasing the AR at presence of moisture and increasing of mechanical load.

Fig. 6 shows the values of STF for different values of AR and mechanical load. It has to be denoted that at smaller AR the values of STF are smaller when the influence of the moisture is taken into account and further increases with the increasing of the mechanical load.

B. Effect of CNF Volume Fracture

Following the definition the CNF volume fraction is defined as the ratio of the CNF to RVE cross-section areas. The CNF volume fraction is varied by varying the matrix width (Fig. 1).

Fig. 7 shows the effect of CNF volume fraction on the distribution of axial shear stresses versus CNF length at $AR = 100$. At this value of AR the plateau length is close to the given CNF length. The results show reduced axial and shear stresses with increased CNF volume fractions.

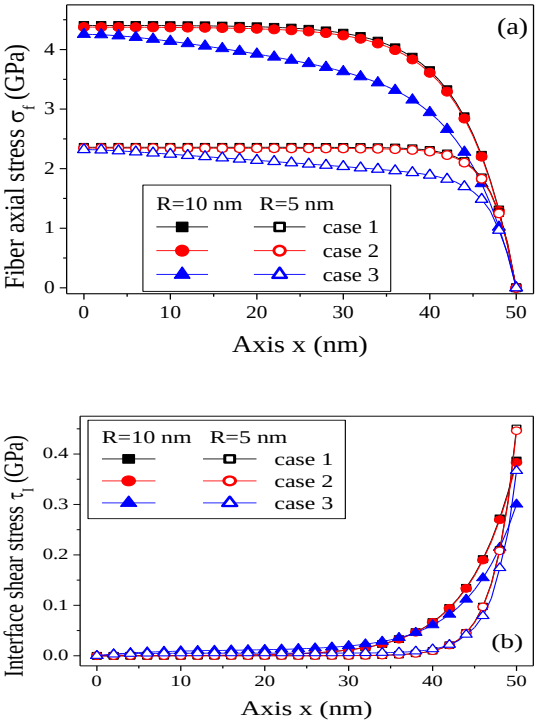

Fig. 7. Effect of CNF volume fraction on axial fiber (a) and interface shear stress (b)

The effect of CNF volume fraction on debond length can be seen on Fig. 8. The results show the decreasing of debond length at the increasing of CNF volume fracture. When the moisture and the applied mechanical load increase the debond length decreases as well.

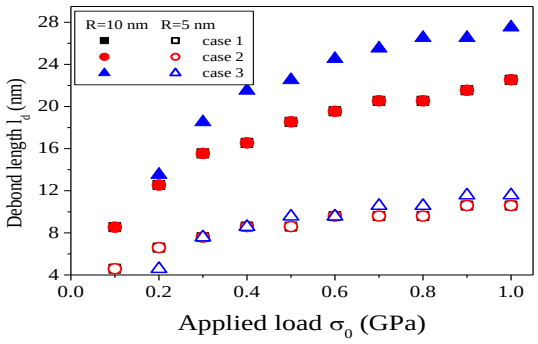

Fig. 8. Effect of CNF volume fraction on debond length

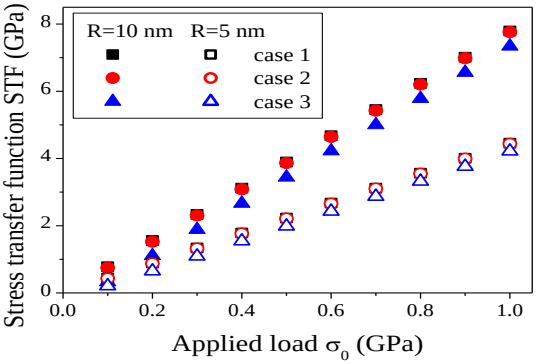

Fig. 9. Effect of CNF volume fraction on values of STF

Fig. 9 shows the effect of CNF volume fraction on values of STF. The values of STF are bigger at smaller CNF volume fraction and increase with increasing the mechanical load. The influence of the moisture on CNF is bigger at smaller volume fraction.

C. Effect of Initial Debond Length

Figures 10-13 show the effect of initial partial debond on the distribution of axial and interface shear stress, debond length, stress transfer function and interface fracture energy along the CNF length.

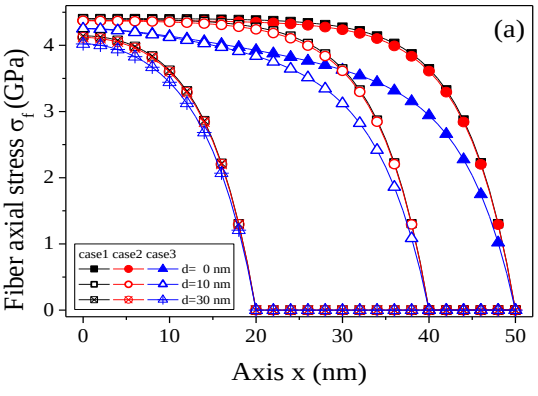

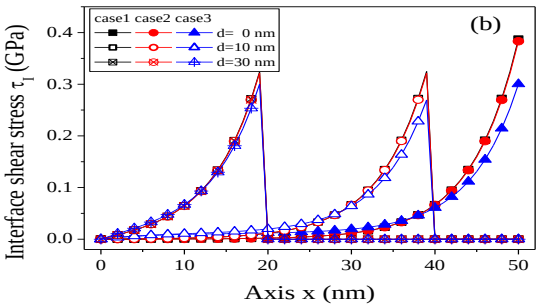

Fig. 10. Effect of initial partial debonding on the fiber axial (a) and interface shear (b) stresses

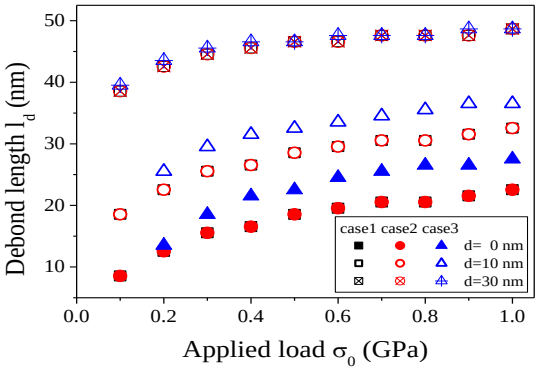

Fig. 11. Effect of initial partial debonding on the debond length

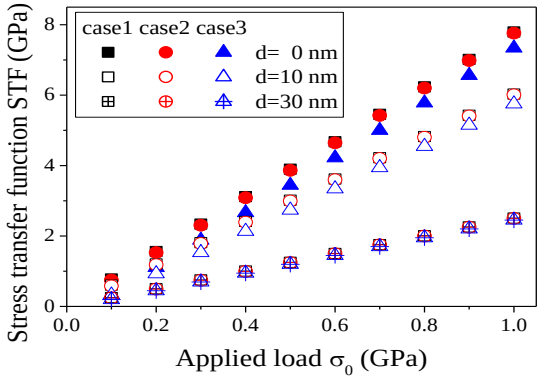

Fig. 12. Effect of initial partial debonding on the stress transfer function

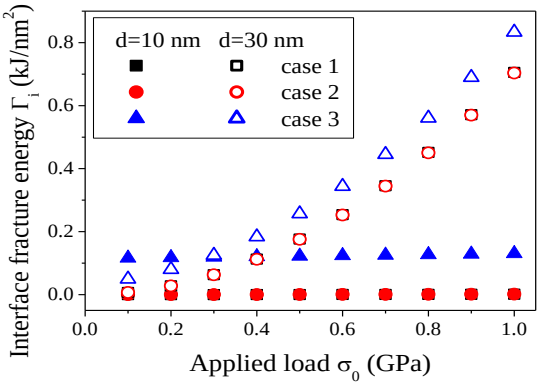

Fig. 13. Effect of initial partial debonding on the interface fracture energy

For this purpose an aspect ratio $AR = 100$ and length of debonding $d = 10, 30\ nm$ are selected. The results show reduced axial and interfacial shear stress (Fig. 10). The presence of the initial partial debond leads to smaller values of the respective fiber axial and interface shear stresses as well as to the magnitude of the plateau of the axial fiber stress (Fig. 10).

The influence of initial partial debond on the progressive debond length, stress transfer function and interface fracture energy is significant (Figs. 11-13). The values of the progressive debond length and interface fracture energy increase with increasing of the initial partial interface debond, mechanical load and moisture (Figs. 11, 13). The values of the stress transfer function also increase with the increasing of the mechanical load, but they decrease with increasing of the initial debond length and appearance of the moisture (Fig. 12). At a given bigger value of the initial partial debonding the influence of the temperature and moisture on the debond length and stress transfer function is negligible.

IV. Conclusion

Following the obtained and illustrated results for the cases 1, 2 and 3 at given mechanical, geometrical and environmental characteristics of CNF composites the respective conclusions can be made:

- As well known, the maximum interfacial shear stress occurs at the fiber end (singularity of interfacial shear stress) and falls to zero along the middle of the fiber. However, the size of plateau of fiber axial stress slowly increases and the maximum values of interfacial shear decreases when the influence of moisture is taken into account.
- The influence of the temperature excitation (20^o-30^oC) at given characteristics of the chosen CNF composite on the interface debond length is negligible, while the influence of moisture is significant especially for the case of progressive interface debonding.
- The values of the progressive debond length and interface fracture energy increase with increasing of the initial partial interface debond, mechanical load and moisture.
- The presence of the initial partial debond leads to smaller values of the respective fiber axial and interface shear stresses as well as to the magnitude of the plateau of the axial fiber stress.
- The influence of the moisture on CNF is bigger at smaller volume fraction.
- At smaller AR the values of STF are smaller when the influence of the moisture is taken into account and further increases with the increasing of the mechanical load.

The results obtained in the present paper could serve for quick prognoses for the interfacial damage behavior of the CNF composites under combine mechanical and physical loading (temperature and moisture) in order to predict their interface damage behavior.

Acknowledgment

The authors acknowledge the financial support of Bulgarian National Foundation E02/10121214 project.

REFERENCES

[1] W. A. Curtin, "Exact theory of fiber fragmentation in a single-filament composite", *J. Mater. Sci*., 26, 1991, 5239-5253.

[2] P. J. Herrera-Franco, R. Venkatesh, L. T. Drzal, "Both strength measurement in composites analysis of experimental techniques", *Composites*, 23, 1992, 2-27.

[3] P. S. Chua, M. R. Piggot, "The glass-fiber-polymer interface: I - Theoretical considerations for single fiber pull-out", *Compos. Sci. Technol.*, 22, 1985, 33-42.

[4] A. Kelly, W. R. Tyson, "Tensile properties of fiber-reinforced metals: copper/tungsten and copper/molybdenum", *J. Mech. Phys. Solids*, 13, 1965, 329-250.

[5] L. T. Drzal, M. J. Rich, P. F. Lloyd, "Adhesion of graphite fibers to epoxy matrices. I. The role of fiber surface treatment", *J. Adhesion*, 16, 1982, 1-30.

[6] J. F. Mandell, D. H. Grande, T.-H. Tsiang, F. J. McGarry, "Modified microdebonding test for direct in situ fiber/matrix bond strength determination in fiber composites", In: *Composite Materials: Testing and Design*, ASTM STP 893, Philadelphia, PA, 1986, 87-108.

[7] A. S. Carrara, F. J. McGarry, "Matrix and interface stresses in a discontinuous fibre composite model", *J. Composite Mater.*, 2(2), 1968, 222-243.

[8] X. L. Chen, Y. J. Liu, "Square representative volume elements for evaluating the effective material properties of carbon nanotube-based composites", *Computational Materials Science*, 29(1), 2004, 1-11.

[9] K. Yazdchi, M. Salehi, "The effects of CNT waviness on interfacial stress transfer characteristics on CNT/polymer composites", *Composites Part A*, 42(10), 2011, 1301-1309.

[10] L. H. Shao, R. Y. Luo, S. L. Bai, J. Wang, "Prediction of effective moduli of carbon nanotube-reinforced composites with waviness and debonding", *Compos. Struct.*, 87(3), 2009, 274-281.

[11] W. K. Ahmed, "Investigation impact of the interfacial debonding on the mechanical properties of nanofiber reinforced composites", *J. Nano- Electron. Phys.*, 5(4), 2013, 04059-1-04059-9.

[12] J. Y. Lui, N. Xu, "Modeling of interface cracks in fibre-reinforced composites with the presence of interphases using the boundary element method", *Mechanics of Materials*, 32(12), 2000, 769-783.

[13] D. Luo, W. X. Wang, Y. Takao, "Effects of the distribution and geometry of carbon nanotubes on the macroscopic stiffness and microscopic stresses of nanocomposites", *Comp. Sci. Tech.*, 67, 2007, 2947-2958 .

[14] H. Hu, L. Onyebueke, A. Abatan, ''Characterizing and modeling mechanical properties of nanocomposites – review and evaluation'', *J. Miner. Mat. Charact. Eng.*, 9(4), 2010, 275-319.

[15] H. L. Cox, "The elasticity and strength of paper and other fibrous materials", *Brit. J. of Applied Physics*, 3, 1952, 72-79.

[16] A. C. Johnson, S. A. Hayes, F. R. Jones, "Data reduction methodologies for single fibre fragmentation test: Role of the interface and interphase", *Composites: Part A*, 40(4), 2009, 449-454.

[17] J. A. Nairn, "On the use of shear-lag methods for analysis of stress transfer in unidirectional composites", *Mech. Mater.*, 26, 1997, 63-80.

[18] A. Haque, A., A. Ramasetty, "Theoretical study of stress transfer in carbon nanotube reinforced polymer matrix composites", *Composite Structures*, 71, 2005, 68-77.

[19] H. D. Wagner, H. D., J. A. Narin, M. Detassis, "Toughness of interfaces from initial fiber-matrix debonding in a single fiber composite fragmentation test", *Appl. Compos. Mater.*, 2, 1995, 107-117.

[20] R. N. Yallee, R. J. Young, "Evaluation of interface fracture energy for single-fibre composites", *Compos. Sci. Technol.*, 58, 1998, 1907-1916.

[21] M. R. Piggot, "Debonding and friction at fibre-polymer interfaces. I: Criteria for failure and sliding", *Compos. Sci. Technol.*, 30, 1987, 295-306.

[22] P. Vaddadi, T. Nakamura, R. S. Singh, "Transient hygrothermal stresses in fiber reinforced composites: a heterogeneous characterization approach", *Composites: Part A*, 34, 2003, 719-730.

Varbinka Valeva is Assoc. Prof., Dr.: Institute of Mechanics, Bulgarian Academy of Sciences, Sofia, Bulgaria. Master Degree Math.: Sofia University, Bulgaria. PhD: Solid Mechanics, Institute for Problems of Mechanics, Russian Academy of Sciences., Moscow, Russia. Mathematical and numerical (BEM) modeling of materials and structures. Over 100 publications.

Jordanka Ivanova is Prof., DSci.: Institute of Mechanics, Bulgarian Academy of Sciences, Sofia, Bulgaria. Master Degree Math.: Harkov State University, Ukraine. PhD: Harkov State University, Ukraine. DSci: Institute of mathematics and informatics, Sofia, Bulgaria. Mathematical modeling of material and structures, nonlinear shell stability. Over 150 publications, 1 monograph, Kluwer, Boston.

Ana Yanakieva is Assoc. Prof., Dr.: Institute of Mechanics, Bulgarian Academy of Sciences, Sofia, Bulgaria. Master Degree Eng.: University of Architecture, Civil Engineering and Geodesy, Sofia, Bulgaria. Contact problems, Coupled Hydro-Mechanical problems, Computer Methods in Mechanics, FEM.